ACSNANO

www.acsnano.org

ARTICLE

Single-Atom Zinc and Anionic Framework as Janus Separator Coatings for Efficient Inhibition of Lithium Dendrites and Shuttle Effect

Chun-Lei Song, Ze-Hui Li, Lin-Yuan Ma, Mian-Zhang Li, Si Huang, Xu-Jia Hong,* Yue-Peng Cai,* and Ya-Qian Lan*

Cite This: https://doi.org/10.1021/acsnano.1c03876

Read Online

ACCESS | Metrics & More | Article Recommendations | Supporting Information

ABSTRACT: The two key problems for the industrialization of Li−S batteries are the dendrite growth of lithium anode and the shuttle effect of lithium polysulfides (LiPSs). Herein, we report the Janus separator prepared by coating anionic Bio-MOF-100 and its derived single-atom zinc catalyst on each side of the Celgard separator. The anionic metal−organic framework (MOF) coating induces the uniform and rapid deposition of lithium ions, while its derived single-atom zinc catalyzes the rapid transformation of LiPSs, thus inhibiting the lithium dendrite and shuttle effect simultaneously. Consequently, compared with other reported Li−S batteries assembled with single-atomic catalysts as separator coatings, our SAZ-AF Janus separator showed stable cyclic performance (0.05% capacity decay rate at 2 C with 1000 cycles), outstanding performance in protecting lithium anode (steady cycle 2800 h at 10 mAh cm^{-2}), and equally excellent cycling performance in Li−SeS_2 or Li−Se batteries. Our work provides an effective separator coating design to inhibit shuttle effect and lithium dendrite.

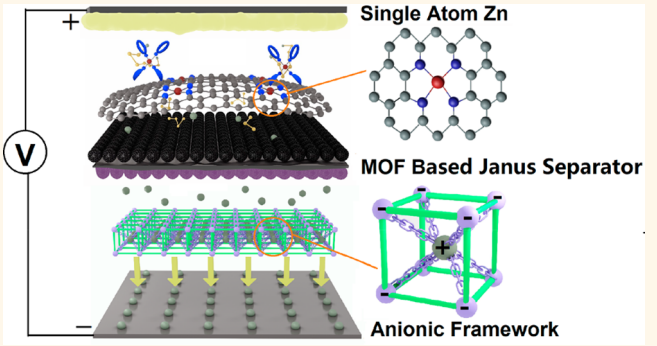

KEYWORDS: *Janus separator, single-atom zinc, metal−organic framework, shuttle effect, lithium dendrite*

Due to their abundant resources, a high theoretical specific capacity (1675 mAh g^{-1}), low cost, and environmental benignity, lithium−sulfur batteries are considered as a promising candidate for the next-generation high-energy density storage devices.[1−4] Despite its bright application prospect, a lithium sulfur battery still faces some unsurpassed challenges in its marketization process at present, with LiPSs shuttle effect and lithium dendrite growth as the two major problems responsible for the cycling instability and poor safety of Li−S batteries, which have become the recent research hotspot and international frontier.[1−8]

Owing to the high activity of lithium metal, the native SEI film formed between electrolyte and lithium metal is usually unstable and fragile during long cycles. It has been reported that the uniform deposition of lithium ion can be promoted by building a functional protective layer or coating on the lithium anode or on the side of the separator facing the lithium anode.[9−14] Compared with traditional porous materials, metal−organic frameworks (MOFs) are characterized with flexible, abundant, and ordered pores, enabling them to screen or transport a variety of ions or molecules effectively. By coating MOFs on the side of the separator facing the lithium anode, the ordered channels of MOFs can enable the lithium ions to be uniformly deposited on the lithium anode, thus inhibiting lithium dendrite growth.[15−20] In this process, the MOFs with the anionic framework can use the charge of their frameworks to promote the rapid and uniform transport of lithium ions.[20−22] Therefore, the uniform and rapid transport of Li^+ ions and inhibition of lithium dendrite growth can be effectively induced by constructing anionic MOFs as the separator coating via selecting MOFs with anionic framework

Received: May 7, 2021
Accepted: August 2, 2021

or transforming the charge of the framework by modifying the ligand and metal nodes.

On the contrary, LiPS shuttle effect can also be effectively suppressed by coating the material on the separator facing the sulfur cathode. So far, many kinds of materials have been applied as separator coatings, such as carbon materials (porous carbon, carbon nanotubes, graphene), metal oxide/sulfide/nitride, and single-atomic catalysts.[23−31] Among them, due to more dispersed and efficient atomic-level catalytic sites, single-atomic catalysts have much better catalytic activity for LiPSs, which can not only catalyze the mutual conversion between insoluble short-chain lithium sulfide ($Li_2S_{(2)}$) and soluble long-chain sulfur (Li_2S_x, $4 \leq x \leq 8$), accelerate the reaction kinetics, and effectively inhibit LiPS shuttle but also reduce the polarization of Li−S battery, thus obtaining excellent cycling performance, especially at a high rate.[32−38]

Therefore, modifying the separator with corresponding functional coating materials is a very simple and effective way to inhibit lithium dendrite growth and LiPS shuttle effect. In this regard, the Janus separator, which is coated with the corresponding functional materials on each side, can solve the two problems efficiently and simultaneously. Thus far, there have been few reports regarding the catalytic conversion of LiPSs in the Janus separator in Li−S batteries, and most of previous studies are based on physical screening or chemisorption, unable to achieve the expected rate performance.[39−47] Additionally, the Janus separator for Li−SeS_2 or Li−Se batteries also face these two problems, and, to our knowledge, few related studies have been performed so far.

Against the above background, the Janus separator was fabricated by using Bio-MOF-100 with an anionic framework and its derived single-atom Zn-decorated embroidered ball-like nitrogen doped carbon (ZnENC) as double-sided coating materials for the separator, named as SAZ-AF Janus separator (Scheme 1). On the one hand, anionic Bio-MOF-100 can

Scheme 1. Scheme of SAZ-AF Janus Separator with Efficient Inhibition of Lithium Dendrites and Shuttle Effect

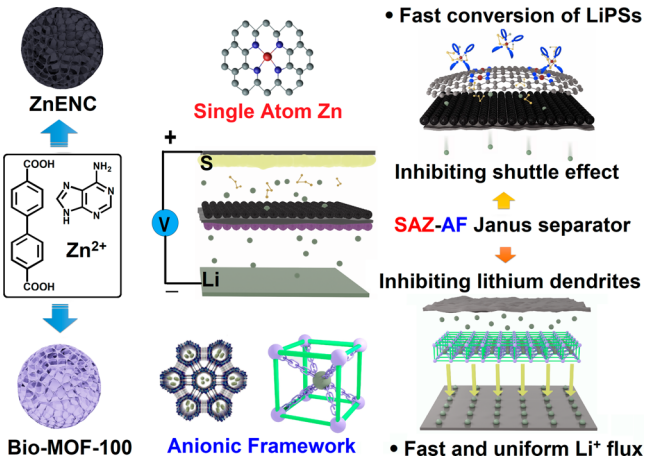

effectively adsorb lithium ions, allowing them to be quickly and uniformly transferred along the ordered channel to the lithium anode to inhibit lithium dendrite growth, achieving an outstanding cycling performance of over 2800 h with a voltage hysteresis of ~55 mV at 5 mA cm^{-2} and 10 mAh cm^{-2} in a Li−Li cell. On the other hand, its derived ZnENC can catalyze LiPS conversion quickly and improve the reaction kinetics to inhibit the shuttle effect, with a cumulative capacity of 240 mAh g^{-1} for Li_2S. As a result, the SAZ-AF Janus separator shows a wide range of applications and could be applied to the Li−S, Li−SeS_2, or Li−Se batteries with excellent cycling performance, which can all work well at a high loading of 4 mg cm^{-2} and a current density of 1−2 C.

RESULTS AND DISCUSSION

In this study, Bio-MOF-100 with nanosize was prepared by dissolving a controlled amount of acetic acid adenine, zinc acetate, BPDC, and CTAB in a solvent mixture of DMF, methanol, and distilled water, followed by stirring and centrifugation to collect a white precipitate. X-ray diffraction (XRD) analysis exhibits complete agreement between the diffraction peaks of the powder and the simulated diffraction peaks of the Bio-MOF-100 reported in previous studies (Figure S1).[48] Scanning electron microscope (SEM) images show that the obtained MOFs were homogeneously embroidered ball-like nanospheres with the uniform honeycomb-like holes on the surface (Figure 1a). After carbonization at 800 °C in argon atmosphere for 8 h, the Bio-MOF-100-derived ZnENC was obtained. As shown in Figure S2a, ZnENC still maintains the morphology of an embroidered ball-

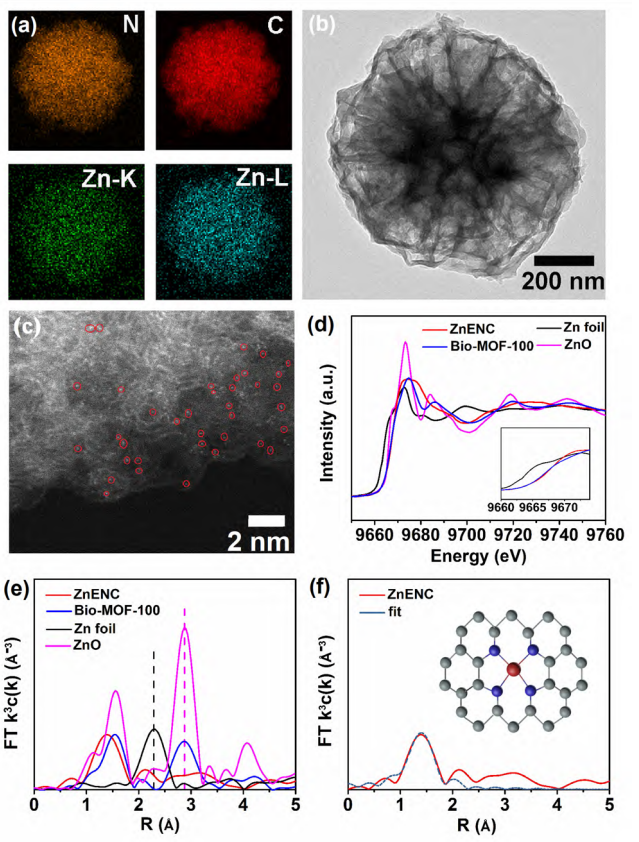

Figure 1. (a) SEM images of Bio-MOF-100. (b) Transmission electron microscopy (TEM) and EDS mapping images of ZnENC. (c) High-angle annular dark-field scanning transmission electron microscopy (HAADF-STEM) observation of ZnENC (with red circles indicating single-atom Zn). (d) Zn K-edge X-ray absorption near edge spectroscopy (XANES) spectra and (e) Fourier transform (FT) of extended X-ray absorption fine structure (EXAFS) spectra (k^3-weight). (f) EXAFS R-space fitting curve of HNCN (inset: ZnENC model, with Zn highlighted in red, N in navy-blue, and C in gray).

https://doi.org/10.1021/acsnano.1c03876
ACS Nano XXXX, XXX, XXX−XXX

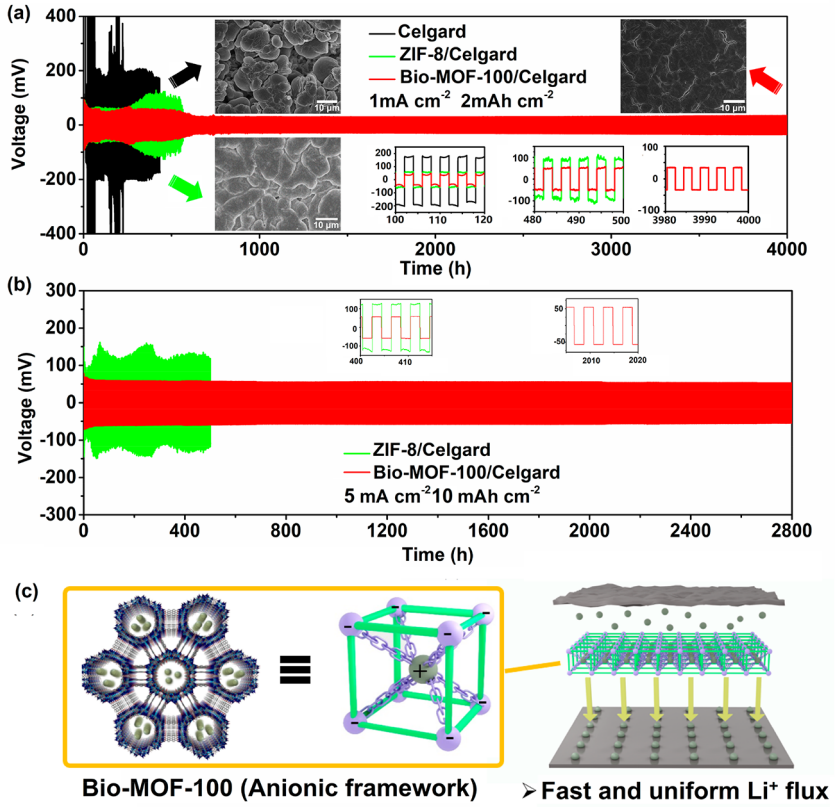

Figure 2. (a) Li plating/stripping behavior at an area capacity of 2 mAh cm^{-2} and the current density of 1 mA cm^{-2} over 4000 h of Li−Li symmetric cells with Celgard separator, ZIF-8/Celgard separator, and 1 Bio-MOF-00/Celgard separator. Inset: SEM images of the lithium film after cycling of symmetric cells with Celgard separator, ZIF-8/Celgard separator, and Bio-MOF-100/Celgard separator. (b) Li plating/stripping behavior in Li−Li symmetric cells with Bio-MOF-100/Celgard and ZIF-8/Celgard separators at 5 mA cm^{-2} and 10 mAh cm^{-2} over 2800 h. (c) Scheme of uniform lithium deposition induced by Bio-MOF-100.

like nanosphere. The XRD test shows that ZnENC is an amorphous carbon material and that Zn has been completely removed at a high temperature without obvious zinc oxide diffraction peaks (Figure S2b). Energy-dispersive X-ray spectroscopy (EDX) mapping indicates that ZnENC is rich in nitrogen and zinc doping (Figure 1b). The X-ray photoelectron spectroscopy (XPS) test shows that the doped nitrogen is of a different structure, including pyrrole nitrogen, pyridine nitrogen, graphite nitrogen, and Zn−N structure formed with zinc (Figure S4).

In XRD test, no zinc oxide or zinc was found in ZnENC (Figure S2b), but ZnENC is rich in zinc, indicating that Zn is distributed on the carbon nanosphere in a smaller size. Additionally, as shown in the transmission electron microscopy (TEM) image of ZnENC in Figure 1b, there are no visible nanoparticles on the carbon nanosphere. All of these results suggest that zinc may be present in ZnENC at the atomic level, which was verified by high-angle annular dark-field scanning transmission electron microscopy (HAADF-STEM)) (Figure 1c). HAADF-STEM analysis shows that Zn elements are widely distributed inside the carbon nanosphere with atomic Zn. The form of Zn species in ZnENC was further investigated by X-ray absorption spectroscopy (XAS), a method commonly used to detect the coordination and the valence status of target atoms. Figure 1d shows the X-ray absorption near-edge structure (XANES) spectrum of ZnENC, which is seen to be located between the spectrum of Bio-MOF-100 and Zn foil, and in the amplified XANES spectra (inset Figure 1d), the adsorption threshold for ZnENC is closer to Bio-MOF-100 rather than Zn foil, suggesting a valence state between 0 and +2 for Zn species in ZnEnc. In Figure 1e, the extended X-ray adsorption fine structure (EXAFS) spectra show that the characteristic peaks of Zn−Zn interactions in Zn foil (2.3 Å) and ZnO (2.9 Å) are absent in ZnENC, while the peak around ∼1.5 Å can be observed in ZnENC, which could be attributed to Zn−N coordination. After fitting EXAFS data to the Zn−N_4 model (inset Figure 1f), Zn−N_4 is shown as the most likely Zn atom's coordination pattern in ZnENC (Figure 1f and Table S1).

From the chemical formula of Bio-MOF-100, $\{[Zn_8(ad)_4(BPDC)_6O_2]\cdot 4Me_2NH_2\}_n$, we can see that it is an ionic MOF, with the anion framework of $\{[Zn_8(ad)_4(BPDC)_6O_2]^{4-}\}_n$ and free-moving cations of $Me_2NH_2^+$ ions in the channels. Whether Bio-MOF-100 is an anionic framework was further confirmed by the adsorption experiments on a series of ionic dyes. As shown in Figure S5, Bio-MOF-100 can quickly adsorb cationic rhodamine B and make the solution clear but shows a poor effect on anionic methylene blue. Thanks to this anionic framework, Bio-MOF-100 coating could induce lithium ions to transfer along the channel, achieving a lithium-ion transfer number of 0.79 (Figures S7−S10).

Whether anionic Bio-MOF-100 can induce the uniform deposition and stripping of Li^+ on lithium metal anode was verified by coating it on Celgard separator to assemble the Li−Li symmetric cells and test the electrochemical performance, using ZIF-8 with the neutral framework as separator coating for comparison. As shown in Figure 2a, the Li−Li symmetric

https://doi.org/10.1021/acsnano.1c03876
ACS Nano XXXX, XXX, XXX−XXX

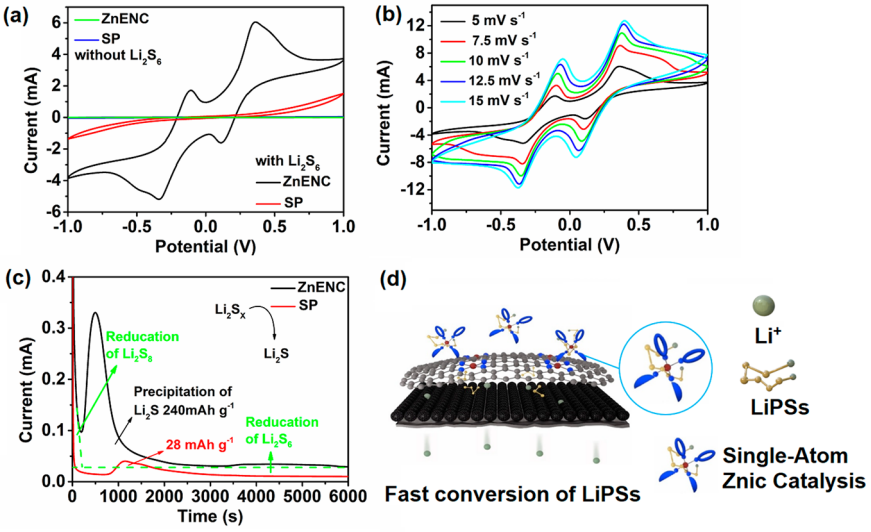

Figure 3. (a) CV curves for the symmetrical cells of ZnENC and SP. (b) CV curves of ZnENC in symmetric cells at a scan rate of 5−15 mV s^{-1}. (c) Potentiostatic discharge curves of the Li_2S_8/tetraglyme solution at 2.05 V on SP or ZnENC. (d) Scheme for inhibiting shuttle effect by ZnENC catalytic conversion of LiPSs.

cell assembled with a common Celgard separator displays a large and unstable polarization voltage of more than 400 mV at 1 mA cm^{-2} and 2 mAh cm^{-2}, while the cell with a ZIF-8/Celgard separator shows a gradually increasing polarization voltage of more than 100 mV after 230 h. In contrast, the polarization voltage of the Li−Li symmetric cell with Bio-MOF-100 coated separator is stable at ∼30 mV and no short circuit occurs even after 4000 h of cycling, which is much better than most previously reported results. After cycling, the cells were disassembled and the surface of lithium metal was tested by SEM. As shown in the inset of Figure 2a, the surface of the lithium metal in the symmetric cell assembled with an ordinary Celgard separator was powdered and a large number of lithium dendrites appeared. For the cell with neutral framework coating, the situation is improving but not satisfactory. However, for the symmetrical cell with Bio-MOF-100 coating, even after cycling for 4000 h, the surface of lithium metal still presents uniform, continuous, and flat lithium without obvious lithium dendrite.

It can be seen that, in the presence of Bio-MOF-100, the excellent ion selectivity of Bio-MOF-100 can greatly benefit the lithium electroplating process under different current densities, thus significantly improving the rate performance of symmetrical cells (Figure S12). Even at 5 mA cm^{-2} and 10 mAh cm^{-2}, the symmetric cell with Bio-MOF-100 coating still exhibits an ultralow polarization voltage of ∼52 mV and a steady cycle of 2800 h (Figure 2b). Besides, the Li−Cu cell with Bio-MOF-100 coating also presents good performance (Figure S13). Collectively, as shown in Figure 2c, the anionic Bio-MOF-100 can effectively adsorb Li^+ ions and enable them to be fast and uniformly transferred along the ordered channel to the lithium anode. The resulted Bio-MOF-100 coating can greatly improve the stability of lithium anode electroplating and stripping process and avoid the generation of lithium dendrites at a high current density, contributing to the commercialization of Li−S batteries.

In order to obtain the separator coating with a high catalytic efficiency for LiPSs to suppress shuttle effect, ZnENC with single-atom Zn catalyst was prepared after the carbonization of Bio-MOF-100. In Figures S14 and S15, the adsorption test and the XPS spectra both indicate strong interaction between single-atom Zn and polysulfide ions. The importance of ZnENC throughout the process of LiPS catalysis was further demonstrated by coating ZnENC and the other contrast samples on aluminum foil as working and pair electrodes and adding LiPSs in the electrolyte to assemble the symmetric cells. The LiPS catalytic strength could be estimated by the intensity of the REDOX peaks. Figure 3a shows the cyclic voltammetry (CV) curves at 5 mV s^{-1} sweep speed and −1.0∼1.0 V voltage range, and no obvious REDOX peaks can be observed in the symmetric cell with SP. However, in the CV curves, the symmetric cell with ZnENC shows two pairs of reversible peaks. The peaks at 0.11 and −0.34 V could be attributed to the process of reducing S_8 to Li_2S_6 and Li_2S_6 to Li_2S, while the peaks at −0.11 and 0.34 V corresponded to the process of oxidizing Li_2S to Li_2S_6 and Li_2S_6 to S_8, respectively. Besides, the Bio-MOF-100-derived single-atomic zinc catalyst has better catalytic performance relative to its derived metal oxides, metal nanoparticles, or metal carbides (Figures S17−S22). Furthermore, due to the electrical conductivity of mesoporous carbon and the electrocatalytic effect of monatomic zinc on LiPSs, the REDOX peaks of the assembled symmetric cell are still extremely obvious even with the scanning rate further increased to 15 mV s^{-1} (Figure 3b).

In addition, the affinity of the polar surface of the material to polysulfides can accelerate the conversion kinetics of LiPSs, which can be measured by thee nucleation/deposition of LiPSs. The nucleation of Li_2S was tested by coating ZnENC and SP to aluminum foil as working electrodes, using lithium foils as pair electrodes and LiPSs as an electrolyte to assemble asymmetric cells. The asymmetric cells were discharged initially at 0.112 mA to 2.06 V, and then, the constant potential remained at 2.05 V until the current fell below 10^{-5} A. This voltage was applied to fully convert the higher order polysulfides, and the deposition rate of Li_2S could be reflected by the integrated area of time and current. In Figure 3c, it is shown that, for the asymmetric cell with ZnENC, Li_2S was transformed immediately after discharge, while the cell with SP began to produce Li_2S after 750 s. The cumulative capacity of the asymmetric cell with ZnENC reached 240 mAh g^{-1}, far

https://doi.org/10.1021/acsnano.1c03876
ACS Nano XXXX, XXX, XXX−XXX

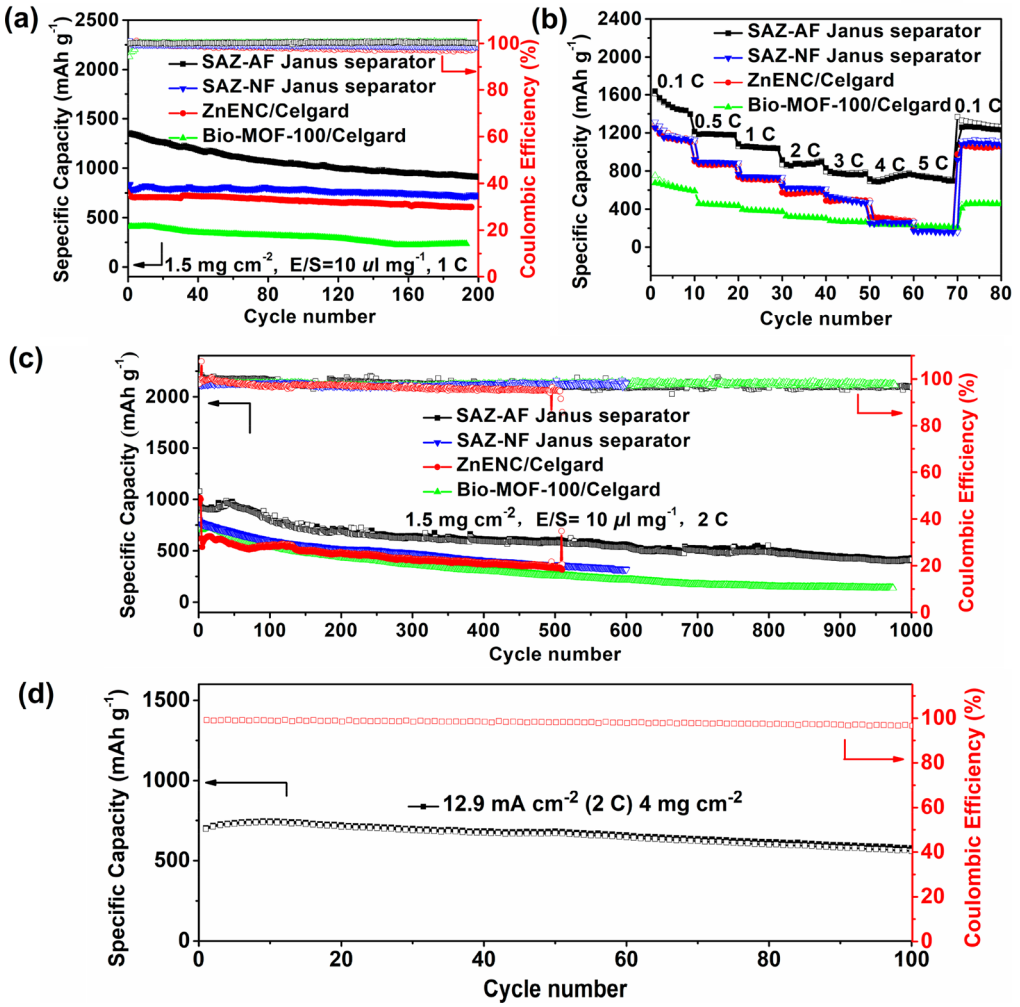

Figure 4. (a) Cycling performance of Li−S cells with various separators at a 1 C rate. (b) Rate performance of Li−S cells with various separators. (c) Cycling performance of Li−S cells with various separators at a 2 C rate over 1000 cycles. (d) Cycling performance of the Li−S cell with the SAZ-AF Janus separator at a 2 C rate and 4 mg cm^{-2} sulfur loading.

higher than the value of only 28 mAh g^{-1} for the cell with SP, further proving that ZnENC could catalyze the conversion of Li_2S_x ($x \geq 4$) to Li_2S quickly and efficiently. Moreover, the working electrodes coated with ZnENC or SP were characterized by SEM after deposition. In Figure S23, a large amount of Li_2S was seen to be uniformly deposited on the surface of ZnENC, while there was almost no Li_2S on the surface of SP. All of these test results show that the mesoporous carbon nanosphere doped with a large amount of single-atom Zn can effectively adsorb LiPSs and catalyze their conversion efficiently, thus effectively suppressing LiPS shuttle effect (Figure 3d).

The above results indicate that anionic Bio-MOF-100 can effectively induce the uniform and fast transport of lithium ions, thus effectively inhibiting lithium dendrite growth even at a high current density. Meanwhile, its derived ZnENC can catalyze LiPS conversion quickly and improve the reaction kinetics. Therefore, these two materials were coated on both sides of the Celgard-2400 separator to prepare the SAZ-AF Janus separator (Figure S24) and applied in a Li−S battery to achieve the effective synergistic inhibition of lithium dendrite and shuttle effect.

The superiority of the SAZ-AF Janus separator in Li−S batteries was tested by assembling a series of Li−S cells with various separators and evaluating their electrochemical performance. Figure 4a displays the cycling performance of Li−S cells with various separators at a 1 C rate and 1.5 mg cm^{-2} sulfur loading. Among them, the SAZ-AF Janus separator cell shows the highest initial specific capacity of 1350 mAh g^{-1}, which is extremely higher than those of the SAZ-NF Janus separator cell (830.1 mAh g^{-1}), ZnENC/Celgard cell (702.5 mAh g^{-1}), and Bio-MOF-100/Celgard cell (405.7 mAh g^{-1}), respectively. Meanwhile, the SAZ-AF Janus separator Li−S cell could retain the specific capacity of 915.1 mAh g^{-1} after 200 cycles, obviously higher than the specific capacity of cells with single coatings to protect the anode or the cathode alone. Figure 4b shows the rate performance of cells assembled with various separators. Among them, the cell with the SAZ-AF Janus separator demonstrates excellent rate performance, with specific capacities of 1651.6, 1209.6, 1092.1, 920.7, 833.5, 707.6, and 701.6 mAh g^{-1} at 0.1, 0.5, 1, 2, 3, 4, and 5 C, respectively. When the current changes from 5 to 0.1 C, the specific capacity can still recover to 1383.9 mAh g^{-1}, which is far higher than those of the cells with other separators. Among them, the ZnENC/Celgard separator failed to protect the lithium anode, making it unable to withstand the cycle under the high current density, while the Bio-MOF-100/Celgard separator failed to suppress the shuttle effect, resulting in a

https://doi.org/10.1021/acsnano.1c03876
ACS Nano XXXX, XXX, XXX−XXX

low-rate performance. However, due to the high catalytic performance of ZnENC coating and effective inhibition of lithium dendrite growth by Bio-MOF-100 coating, the cell with the SAZ-AF Janus separator has an excellent rate performance, with a clear charging and discharging platform being still visible at 5 C, as shown in Figure S29. Besides, for Janus separators, the cells with anionic framework coating present much better performance compared with the neutral framework coating for lithium metal anode. The effects of SAZ-AF Janus separator in suppressing LiPS shuttle effect and protecting lithium anode were further verified by disassembling the cells with different separators operated at 1 C after 100 cycles (Figure S33). The results further confirmed the effectiveness of the single-atomic Zn and anionic framework as a Janus separator coating in protecting lithium anode and inhibiting shuttle effect.

Furthermore, the long-cycle stability of the cells at a high current density was tested. In Figure 4c, it was shown that, despite a reasonable discharge capacity of the cell with ZnENC/Celgard in the first cycle, the lithium anode cannot withstand a long cycle at a large current, causing lithium dendrites to puncture the separator and the specific capacity of the cell to decrease fast with a 0.1% capacity decay per cycle and only 339 mAh g^{-1} after 500 cycles. For the cell with Bio-MOF-100/Celgard, the coating of MOF could inhibit lithium dendrite growth, thus greatly increasing the cycle life to more than 900 cycles. However, it cannot effectively catalyze the conversion of lithium polysulfides, making the specific capacity far lower than the theoretical specific capacity. After 977 cycles, the specific capacity was only 120.9 mAh g^{-1}. The application of Janus separator in the neutral framework of ZIF-8 as the coating facing lithium anode still failed to improve the cell performance. Only the Li−S cell with a Janus separator based on single-atom zinc and anionic framework coating displays an excellent performance with an initial specific capacity of 943.5 mAh g^{-1} at 2 C. Even after 1000 cycles, a specific capacity of 424.3 mAh g^{-1} could be still maintained with 0.05% capacity decay per cycle. Even in the case of higher sulfur loadings of 3, 5, or 8 mg cm^{-2}, the SAZ-AF Janus separator could still play an effective function, with area capacities of 3.6, 5.6, and 6.8 mAh cm^{-2}, respectively (Figure S34). Moreover, even at 12.9 mA cm^{-2} current density and 4 mg/cm^2 sulfur loading, the cell with the SAZ-AF Janus separator showed an excellent performance of 694.8 mAh g^{-1} initial capacity, which can be still maintained at 564.7 mAh g^{-1} after 100 cycles (Figure 4d). Compared with the reported separators based on single-atom catalyst coating or other Janus separators, our SAZ-AF Janus separator displays better performance (Figures S41−S43).

In a Li−S battery, the SAZ-AF Janus separator was shown to effectively suppress shuttle effect and lithium dendrite growth. Considering that the Li−SeS_2 battery and Li−Se battery also face these two problems, we further used the SAZ-AF Janus separator in these two batteries to explore its application universality. Results show that the SAZ-AF Janus separator can protect both cathode and anode and is suitable for Li−S, Li−Se, and Li−SeS_2 batteries with a high-rate performance and a stable long cycle for all the three types of batteries (Figures S35−S40, Tables S2−S4).

CONCLUSION

In this study, a SAZ-AF Janus separator was prepared by using a MOF-derived monatomic catalyst with efficient catalytic function for LiPSs and the anionic MOF with rapid lithium-ion conduction and efficient inhibition of lithium dendrite growth as double-sided coating materials. The single-atomic zinc shows superior catalytic performance to metal oxides, metal nanoparticles, or metal carbides, and the Li−Li symmetric cell assembled with Bio-MOF-100 coating could cycle steadily for 2800 h at 5 mA cm^{-2} and 10 mAh cm^{-2}, with far better performance than those of most previously reported separator coatings. The resulting SAZ-AF Janus separator achieved outstanding performance in different Li−S batteries assembled with single-atomic catalysts as separator coatings (0.05% capacity decay rate at 2 C and 1000 cycles) and showed superior performance in protecting lithium anode (steadily cycling at 10 mAh cm^{-2} for 2800 h). This report provides a facile method for preparing the high-performance functional separator with wide applications.

EXPERIMENTAL SECTION

Preparation of Bio-MOF-100. Briefly, adenine (0.134 g) and 4,4-biphenyl dicarboxylic acid (BPDC) (0.48 g) were dissolved separately in 20 mL of *N*,*N*-dimethylformamide (DMF), followed by dissolving zincacetate (0.42 g) and polyvinyl prrrolidone (PVP, 2 g) in 40 mL of DMF. After being completely dissolved by ultrasound for 10 min, the above solutions were supplemented with 20 mL of DMF, 4 mL of methanol, and 2 mL of deionized water, followed by stirring at room temperature for 18 h, centrifugation to collect the precipitate, and drying to obtain a white powder as Bio-MOF-100.

Fabrication of ZnENC, Bio-MOF-100-600, and Bio-MOF-100-700. Briefly, ZnENC, a black powder, was prepared by carbonizing Bio-MOF-100 for 8 h under an argon environment at 800 and 5 °C/min, and the same method was used to prepare Bio-MOF-100−600 and Bio-MOF-100−700 by replacing 800 °C with 600 and 700 °C, respectively.

Fabrication of Zn/Co-Bio-MOF-100, Zn/Fe-Bio-MOF-100, and Zn/Ni-Bio-MOF-100. Briefly, BPDC (0.48 g) and adenine (0.134 g) were dissolved separately in 20 mL of DMF, followed by dissolving cobalt acetate (0.028 g), polyvinyl prrrolidone (PVP, 2 g), and zinc acetate (0.39 g) separately in 40 mL of DMF. After being completely dissolved by ultrasound for 10 min, the above solutions were supplemented with 20 mL of DMF, 4 mL of methanol, and 2 mL of deionized water, followed by stirring at room temperature for 18 h, centrifugation to collect the precipitate, and drying to obtain a pink powder as Zn/Co-Bio-MOF-100. As described above, Zn/Fe-Bio-MOF-100 and Zn/Ni-Bio-MOF-100 were prepared by replacing cobalt acetate with ferric chloride or nickel acetate, respectively.

Preparation of SAZ-AF Janus Separator, SAZ-NF Janus Separator, ZnENC, Bio-MOF-100, Bio-MOF-100-Derived Co, Fe_3C, $Ni_3ZnC_{0.7}$/Ni, ZnO, and Super-P (SP) Coated Separators. For the ZnENC coated separator (ZnENC/Celgard), ZnENC, Super P, and poly(vinylidene fluoride) (PVDF) were mixed together at a weight ratio of 6:2:2 followed by adding a suitable amount of *N*-methyl pyrrolidone (NMP), stirring, and coating the obtained homogeneous slurry uniformly on one side of Celgard-2400 separator by using a doctor-blade coating process. After drying in a vacuum oven at 60 °C for 12 h, the obtained ZnENC coated separator was cut into 19 mm diameter discs. The same method was used to prepare Bio-MOF-100, Bio-MOF-100-derived Co, Fe_3C, $Ni_3ZnC_{0.7}$/Ni, ZnO, and SP coated separators, named as Bio-MOF-100/Celgard, Co/Celgard, Fe_3C/Celgard, $Ni_3ZnC_{0.7}$/Ni/Celgard, ZnO/Celgard, and SP/Celgard separators.

The SAZ-NF Janus separator was prepared by coating the slurry of single-atom zinc (ZnENC) and ZIF-8 with a neutral framework on each side of the Celgard-2400 separator.

The SAZ-AF Janus separator was prepared by coating the slurry of single-atom zinc (ZnENC) and Bio-MOF-100 with an anionic framework on each side of the Celgard-2400 separator, with the weight of the Janus coating materials adjusted to ~0.1 mg/cm^2, which will not produce much impact on the overall energy density of the battery.

https://doi.org/10.1021/acsnano.1c03876
ACS Nano XXXX, XXX, XXX−XXX

ASSOCIATED CONTENT

Supporting Information

The Supporting Information is available free of charge at https://pubs.acs.org/doi/10.1021/acsnano.1c03876.

Discussions of synthesis methods, visible adsorption of LiPSs, assembly and measurements of Li_2S_6-based symmetric cell, Li_2S nucleation test experiment, test of Li^+ transfer number, electrochemical measurements, characterization, electrocatalytic performance, and performance of the Li−SeS_2 cells and Li−Se cell with different separators, figures of PXRD spectra, SEM and TEM images, N_2 adsorption−desorption isotherm, XPS spectra, adsorption tests, impedance spectra, EIS spectra, comparison of Li plating/stripping behavior, Coulomb efficiency, XRD patterns, CV curves, photograph of the SAZ-AF Janus separator, cycling performance, rate performance, discharge/charge profiles, EIS curves, photographs of the surfaces of the different separators, comparison of single-atoms catalyst, and comparison of Janus separators, and tables of EXAFS fitting parameters, comparison of Janus separators, comparison of single-atoms catalysts, performance comparison of the Li−SeS_2 batteries, performance comparison of the Li−Se batteries, and ICP data of Zn in ZnENC (PDF)

AUTHOR INFORMATION

Corresponding Authors

Xu-Jia Hong − *School of Chemistry, South China Normal University, Guangzhou 510006, P. R. China; School of Pharmaceutical Sciences, Guangzhou Medical University, Guangzhou 511436, P. R. China;* orcid.org/0000-0001-9464-9799; Email: hxuscnu@m.scnu.edu.cn

Yue-Peng Cai − *School of Chemistry, South China Normal University, Guangzhou 510006, P. R. China*; Email: caiyp@scnu.edu.cn

Ya-Qian Lan − *School of Chemistry, South China Normal University, Guangzhou 510006, P. R. China;* orcid.org/0000-0002-2140-7980; Email: yqlan@njnu.edu.cn

Authors

Chun-Lei Song − *School of Chemistry, South China Normal University, Guangzhou 510006, P. R. China*

Ze-Hui Li − *School of Chemistry, South China Normal University, Guangzhou 510006, P. R. China*

Lin-Yuan Ma − *School of Chemistry, South China Normal University, Guangzhou 510006, P. R. China*

Mian-Zhang Li − *School of Chemistry, South China Normal University, Guangzhou 510006, P. R. China*

Si Huang − *School of Chemistry, South China Normal University, Guangzhou 510006, P. R. China*

Complete contact information is available at: https://pubs.acs.org/10.1021/acsnano.1c03876

Author Contributions

All authors contributed to the writing of this manuscript.

Notes

The authors declare no competing financial interest.

ACKNOWLEDGMENTS

Financial support for this work includes the National Natural Science Foundation of P. R. China (Grant No. 22001082), Guangdong Basic and Applied Basic Research Fund Project (2019B1515120027); Research and Development (R&D) Projects in Key Areas of Guangdong Province (2020B0101028005), Guangdong Natural Science Foundation Project (No. 2019A1515010841), Guangdong Province International Science and Technology Cooperation Project (No. 2019A050510038), and Guangzhou Science and Technology Association Young Talents Promotion Project (No. X20210201043); Basic and Applied Basic Research Projects of Guangzhou (No. 202102020624).

REFERENCES

(1) Yu, X.; Manthiram, A. A Progress Report on Metal−Sulfur Batteries. *Adv. Funct. Mater.* **2020**, *30* (39), 2004084.

(2) Wang, R.; Luo, C.; Wang, T.; Zhou, G.; Deng, Y.; He, Y.; Zhang, Q.; Kang, F.; Lv, W.; Yang, Q.-H. Bidirectional Catalysts for Liquid−Solid Redox Conversion in Lithium−Sulfur Batteries. *Adv. Mater.* **2020**, *32* (32), 2000315.

(3) Yang, X.; Luo, J.; Sun, X. Towards High-Performance Solid-State Li−S Batteries: From Fundamental Understanding to Engineering Design. *Chem. Soc. Rev.* **2020**, *49* (7), 2140−2195.

(4) Zhou, H.-J.; Song, C.-L.; Si, L.-P.; Hong, X.-J.; Cai, Y.-P. The Development of Catalyst Materials for the Advanced Lithium-Sulfur Battery. *Catalysts* **2020**, *10* (6), 682.

(5) Hong, X.-J.; Song, C.-L.; Yang, Y.; Tan, H.-C.; Li, G.-H.; Cai, Y.-P.; Wang, H. Cerium Based Metal-Organic Frameworks as an Efficient Separator Coating Catalyzing the Conversion of Polysulfides for High Performance Lithium-Sulfur Batteries. *ACS Nano* **2019**, *13* (2), 1923−1931.

(6) Li, G.; Lu, F.; Dou, X.; Wang, X.; Luo, D.; Sun, H.; Yu, A.; Chen, Z. Polysulfide Regulation by the Zwitterionic Barrier toward Durable Lithium−Sulfur Batteries. *J. Am. Chem. Soc.* **2020**, *142* (7), 3583−3592.

(7) Lee, D. K.; Chae, Y.; Yun, H.; Ahn, C. W.; Lee, J. W. CO_2-Oxidized $Ti_3C_2T_x$−MXenes Components for Lithium−Sulfur Batteries: Suppressing the Shuttle Phenomenon through Physical and Chemical Adsorption. *ACS Nano* **2020**, *14* (8), 9744−9754.

(8) Gu, J.; Zhu, Q.; Shi, Y.; Chen, H.; Zhang, D.; Du, Z.; Yang, S. Single Zinc Atoms Immobilized on MXene ($Ti_3C_2Cl_x$) Layers toward Dendrite-Free Lithium Metal Anodes. *ACS Nano* **2020**, *14* (1), 891−898.

(9) Yao, W.; Zheng, W.; Xu, J.; Tian, C.; Han, K.; Sun, W.; Xiao, S. ZnS-SnS@NC Heterostructure as Robust Lithiophilicity and Sulfiphilicity Mediator toward High-Rate and Long-Life Lithium−Sulfur Batteries. *ACS Nano* **2021**, *15* (4), 7114−7130.

(10) Liu, D.-H.; Bai, Z.; Li, M.; Yu, A.; Luo, D.; Liu, W.; Yang, L.; Lu, J.; Amine, K.; Chen, Z. Developing High Safety Li-metal Anodes for Future High-Energy Li-Metal Batteries: Strategies and Perspectives. *Chem. Soc. Rev.* **2020**, *49* (15), 5407−5445.

(11) Hu, M.; Ma, Q.; Yuan, Y.; Pan, Y.; Chen, M.; Zhang, Y.; Long, D. Grafting Polyethyleneimine on Electrospun Nanofiber Separator to Stabilize Lithium Metal Anode for Lithium Sulfur Batteries. *Chem. Eng. J.* **2020**, *388*, 124258.

(12) Yue, H.; Zhu, Q.; Dong, S.; Zhou, Y.; Yang, Y.; Cheng, L.; Qian, M.; Liang, L.; Wei, W.; Wang, H. Nanopile Interlocking Separator Coating toward Uniform Li Deposition of the Li Metal Anodes. *ACS Appl. Mater. Interfaces* **2020**, *12* (39), 43543−43552.

(13) Liang, J.; Chen, Q.; Liao, X.; Yao, P.; Zhu, B.; Lv, G.; Wang, X.; Chen, X.; Zhu, J. A Nano-Shield Design for Separators to Resist Dendrite Formation in Lithium-Metal Batteries. *Angew. Chem., Int. Ed.* **2020**, *59* (16), 6561−6566.

(14) Wang, X.; Kerr, R.; Chen, F.; Goujon, N.; Pringle, J. M.; Mecerreyes, D.; Forsyth, M.; Howlett, P. C. Toward High-Energy-Density Lithium Metal Batteries: Opportunities and Challenges for Solid Organic Electrolytes. *Adv. Mater.* **2020**, *32* (18), 1905219.

(15) Liu, W.; Mi, Y.; Weng, Z.; Zhong, Y.; Wu, Z.; Wang, H. Functional Metal−Organic Framework Boosting Lithium Metal Anode Performance *via* Chemical Interactions. *Chemical Science.* **2017**, *8* (6), 4285−4291.

(16) Bai, S.; Sun, Y.; Yi, J.; He, Y.; Qiao, Y.; Zhou, H. High-Power Li-Metal Anode Enabled by Metal-Organic Framework Modified Electrolyte. *Joule.* **2018**, *2* (10), 2117−2132.
(17) Zhong, Y.; Lin, F.; Wang, M.; Zhang, Y.; Ma, Q.; Lin, J.; Feng, Z.; Wang, H. Metal Organic Framework Derivative Improving Lithium Metal Anode Cycling. *Adv. Funct. Mater.* **2020**, *30* (10), 1907579.
(18) Qian, J.; Li, Y.; Zhang, M.; Luo, R.; Wang, F.; Ye, Y.; Xing, Y.; Li, W.; Qu, W.; Wang, L.; Li, L.; Li, Y.; Wu, F.; Chen, R. Protecting Lithium/Sodium Metal Anode with Metal-Organic Framework Based Compact and Robust Shield. *Nano Energy* **2019**, *60*, 866−874.
(19) He, J.; Chen, Y.; Manthiram, A. Vertical Co_9S_8 Hollow Nanowall Arrays Grown on a Celgard Separator as a Multifunctional Polysulfide Barrier for High-Performance Li−S Batteries. *Energy Environ. Sci.* **2018**, *11* (9), 2560−2568.
(20) Xu, W.; Pei, X.; Diercks, C. S.; Lyu, H.; Ji, Z.; Yaghi, O. M. A Metal−Organic Framework of Organic Vertices and Polyoxometalate Linkers as a Solid-State Electrolyte. *J. Am. Chem. Soc.* **2019**, *141* (44), 17522−17526.
(21) Zhu, F.; Bao, H.; Wu, X.; Tao, Y.; Qin, C.; Su, Z.; Kang, Z. High-Performance Metal−Organic Framework-Based Single Ion Conducting Solid-State Electrolytes for Low-Temperature Lithium Metal Batteries. *ACS Appl. Mater. Interfaces* **2019**, *11* (46), 43206−43213.
(22) Chiochan, P.; Yu, X.; Sawangphruk, M.; Manthiram, A. A Metal Organic Framework Derived Solid Electrolyte for Lithium−Sulfur Batteries. *Adv. Energy Mater.* **2020**, *10* (27), 2001285.
(23) Jiang, G.; Li, K.; Yu, F.; Li, X.; Mao, J.; Jiang, W.; Sun, F.; Dai, B.; Li, Y. Robust Artificial Solid-Electrolyte Interfaces with Biomimetic Ionic Channels for Dendrite-Free Li Metal Anodes. *Adv. Energy Mater.* **2021**, *11* (6), 2003496.
(24) Zeng, P.; Liu, C.; Zhao, X.; Yuan, C.; Chen, Y.; Lin, H.; Zhang, L. Enhanced Catalytic Conversion of Polysulfides Using Bimetallic Co_7Fe_3 for High-Performance Lithium−Sulfur Batteries. *ACS Nano* **2020**, *14* (9), 11558−11569.
(25) Yang, Y.; Hong, X.-J.; Song, C.-L.; Li, G.-H.; Zheng, Y.-X.; Zhou, D.-D.; Zhang, M.; Cai, Y.-P.; Wang, H. Lithium Bis-(trifluoromethanesulfonyl)imide Assisted Dual-Functional Separator Coating Materials Based on Covalent Organic Frameworks for High-Performance Lithium-Selenium Sulfide Batteries. *J. Mater. Chem. A* **2019**, *7* (27), 16323−16329.
(26) Zhang, N.; Li, B.; Li, S.; Yang, S. Mesoporous Hybrid Electrolyte for Simultaneously Inhibiting Lithium Dendrites and Polysulfide Shuttle in Li−S Batteries. *Advanced Energy Materials.* **2018**, *8* (16), 1703124.
(27) Tu, S.; Chen, X.; Zhao, X.; Cheng, M.; Xiong, P.; He, Y.; Zhang, Q.; Xu, Y. A Polysulfide-Immobilizing Polymer Retards the Shuttling of Polysulfide Intermediates in Lithium−Sulfur Batteries. *Adv. Mater.* **2018**, *30* (45), 1804581.
(28) Hong, X.-J.; Song, C.-L.; Wu, Z.-M.; Li, Z.-H.; Cai, Y.-P.; Wang, C.-X.; Wang, H. Sulfophilic and Llithophilic Sites in Bimetal Nickel-Zinc Carbide with Fast Conversion of Polysulfides for High-Rate Li-S Battery. *Chem. Eng. J.* **2021**, *404*, 126566.
(29) Pang, Y.; Wei, J.; Wang, Y.; Xia, Y. Synergetic Protective Effect of the Ultralight MWCNTs/NCQDs Modified Separator for Highly Stable Lithium−Sulfur Batteries. *Advanced Energy Materials.* **2018**, *8* (10), 1702288.
(30) Pei, F.; Lin, L.; Fu, A.; Mo, S.; Ou, D.; Fang, X.; Zheng, N. A Two-Dimensional Porous Carbon-Modified Separator for High-Energy-Density Li-S Batteries. *Joule.* **2018**, *2* (2), 323−336.
(31) He, J.; Chen, Y.; Manthiram, A. Vertical Co9S8 Hollow Nanowall Arays Grown on a Celgard Separator as a Multifunctional Polysulfide Barrier for High-Performance Li−S Batteries. *Energy Environ. Sci.* **2018**, *11* (9), 2560−2568.
(32) Song, C.-L.; Li, Z.-H.; Li, M.-Z.; Huang, S.; Hong, X.-J.; Si, L.-P.; Zhang, M.; Cai, Y.-P. Iron Carbide Dispersed on Nitrogen-Doped Graphene-Like Carbon Nanosheets for Fast Conversion of Polysulfides in Li−S Batteries. *ACS Applied Nano Materials.* **2020**, *3* (10), 9686−9693.
(33) Yang, Q.; Yang, C.-C.; Lin, C.-H.; Jiang, H.-L. Metal−Organic-Framework-Derived Hollow *N*-Doped Porous Carbon with Ultrahigh Concentrations of Single Zn Atoms for Efficient Carbon Dioxide Conversion. *Angew. Chem., Int. Ed.* **2019**, *58* (11), 3511−3515.
(34) Song, Z.; Zhang, L.; Doyle-Davis, K.; Fu, X.; Luo, J.-L.; Sun, X. Recent Advances in MOF-Derived Single Atom Catalysts for Electrochemical Applications. *Adv. Energy Mater.* **2020**, *10* (10), 2001561.
(35) Xie, J.; Li, B.-Q.; Peng, H.-J.; Song, Y.-W.; Zhao, M.; Chen, X.; Zhang, Q.; Huang, J.-Q. Implanting Atomic Cobalt within Mesoporous Carbon toward Highly Stable Lithium−Sulfur Batteries. *Adv. Mater.* **2019**, *31* (43), 1903813.
(36) Lu, C.; Chen, Y.; Yang, Y.; Chen, X. Single-Atom Catalytic Materials for Lean-Electrolyte Ultrastable Lithium−Sulfur Batteries. *Nano Lett.* **2020**, *20* (7), 5522−5530.
(37) Zhang, K.; Chen, Z.; Ning, R.; Xi, S.; Tang, W.; Du, Y.; Liu, C.; Ren, Z.; Chi, X.; Bai, M.; Shen, C.; Li, X.; Wang, X.; Zhao, X.; Leng, K.; Pennycook, S. J.; Li, H.; Xu, H.; Loh, K. P.; Xie, K. Single-Atom Coated Separator for Robust Lithium−Sulfur Batteries. *ACS Appl. Mater. Interfaces* **2019**, *11* (28), 25147−25154.
(38) Zhou, G.; Zhao, S.; Wang, T.; Yang, S.-Z.; Johannessen, B.; Chen, H.; Liu, C.; Ye, Y.; Wu, Y.; Peng, Y.; Liu, C.; Jiang, S. P.; Zhang, Q.; Cui, Y. Theoretical Calculation Guided Design of Single-Atom Catalysts toward Fast Kinetic and Long-Life Li−S Batteries. *Nano Lett.* **2020**, *20* (2), 1252−1261.
(39) Chen, M.; Chen, Z.; Fu, X.; Zhong, W.-H. A Janus Protein-Based Nanofabric for Trapping Polysulfides and Stabilizing Lithium Metal in Lithium−Sulfur Batteries. *J. Mater. Chem. A* **2020**, *8* (15), 7377−7389.
(40) Peng, H.-J.; Wang, D.-W.; Huang, J.-Q.; Cheng, X.-B.; Yuan, Z.; Wei, F.; Zhang, Q. Janus Separator of Polypropylene-Supported Cellular Graphene Framework for Sulfur Cathodes with High Utilization in Lithium−Sulfur Batteries. *Advanced Science.* **2016**, *3* (1), 1500268.
(41) Zhou, Z.; Chen, B.; Fang, T.; Li, Y.; Zhou, Z.; Wang, Q.; Zhang, J.; Zhao, Y. A Multifunctional Separator Enables Safe and Durable Lithium/Magnesium−Sulfur Batteries under Elevated Temperature. *Adv. Energy Mater.* **2020**, *10* (5), 1902023.
(42) Xu, L.; Daphne Ma, X. Y.; Wang, W.; Liu, J.; Wang, Z.; Lu, X. Polymeric One-Side Conductive Janus Separator with Preferably Oriented Pores for Enhancing Lithium Metal Battery Safety. *J. Mater. Chem. A* **2021**, *9* (6), 3409−3417.
(43) Kim, S.; Lim, W.-G.; Cho, A.; Jeong, J.; Jo, C.; Kang, D.; Han, S. M.; Han, J. W.; Lee, J. Simultaneous Suppression of Shuttle Effect and Lithium Dendrite Growth by Lightweight Bifunctional Separator for Li−S Batteries. *ACS Applied Energy Materials.* **2020**, *3* (3), 2643−2652.
(44) He, Y.; Chang, Z.; Wu, S.; Qiao, Y.; Bai, S.; Jiang, K.; He, P.; Zhou, H. Simultaneously Inhibiting Lithium Dendrites Growth and Polysulfides Shuttle by a Flexible MOF-Based Membrane in Li−S Batteries. *Advanced Energy Materials.* **2018**, *8* (34), 1802130.
(45) Yang, Y.; Wang, W.; Li, L.; Li, B.; Zhang, J. Stable Cycling of Li−S Batteries by Simultaneously Suppressing Li-dendrite Growth and Polysulfide Shuttling Enabled by a Bioinspired Separator. *J. Mater. Chem. A* **2020**, *8* (7), 3692−3700.
(46) Wang, J.; Yi, S.; Liu, J.; Sun, S.; Liu, Y.; Yang, D.; Xi, K.; Gao, G.; Abdelkader, A.; Yan, W.; Ding, S.; Kumar, R. V. Suppressing the Shuttle Effect and Dendrite Growth in Lithium−Sulfur Batteries. *ACS Nano* **2020**, *14* (8), 9819−9831.
(47) Deng, N.; Wang, L.; Feng, Y.; Liu, M.; Li, Q.; Wang, G.; Zhang, L.; Kang, W.; Cheng, B.; Liu, Y. Co-Based and Cu-Based MOFs Modified Separators to Strengthen the Kinetics of Redox Reaction and Inhibit Lithium-Dendrite for Long-Life Lithium-Sulfur Batteries. *Chem. Eng. J.* **2020**, *388*, 124241.
(48) An, J.; Farha, O. K.; Hupp, J. T.; Pohl, E.; Yeh, J. I.; Rosi, N. L. Metal-Adeninate Vertices for the Construction of an Exceptionally Porous Metal-Organic Framework. *Nat. Commun.* **2012**, *3* (1), 604.

https://doi.org/10.1021/acsnano.1c03876
ACS Nano XXXX, XXX, XXX−XXX